Self-Assembly of Large-Scale and Ultrathin Silver Nanoplate Films with Tunable Plasmon Resonance Properties

Xiao-Yang Zhang,[†] Anming Hu,[†,‡,*] Tong Zhang,[†,*] Wei Lei,[†] Xiao-Jun Xue,[†] Yunhong Zhou,[‡] and Walt W. Duley[§]

[†]School of Electronic Science and Engineering, Southeast University, and Key Laboratory of Micro-Inertial Instrument and Advanced Navigation Technology, Ministry of Education, Nanjing, 210096, China, [‡]Department of Mechanical and Mechatronics Engineering, University of Waterloo, 200 University Avenue West, Waterloo, Ontario N2L 3G1, Canada, and [§]Department of Physics and Astronomy, University of Waterloo, 200 University Avenue West, Waterloo, Ontario, N2L 3G1, Canada

ABSTRACT We describe a rapid, simple, room-temperature technique for the production of large-scale metallic thin films with tunable plasmonic properties assembled from size-selected silver nanoplates (SNPs). We outline the properties of a series of ultrathin monolayer metallic films (8−20 nm) self-assembled on glass substrates in which the localized surface plasmon resonance can be tuned over a range from 500 to 800 nm. It is found that the resonance peaks of the films are strongly dependent on the size of the nanoplates and the refractive index of the surrounding dielectric. It is also shown that the bandwidth and the resonance peak of the plasmon resonance spectrum of the metallic films can be engineered by simply controlling aggregation of the SNP. A three-dimensional finite element method was used to investigate the plasmon resonance properties for individual SNPs in different dielectrics and plasmon coupling in SNP aggregates. A 5−17 times enhancement of scattering from these SNP films has been observed experimentally. Our experimental results, together with numerical simulations, indicate that this self-assembly method shows great promise in the production of nanoscale metallic films with enormous electric-field enhancements at visible and near-infrared wavelengths. These may be utilized in biochemical sensing, solar photovoltaic, and optical processing applications.

KEYWORDS: plasmonics · silver nanoplates · localized surface plasmon resonance · scattering light · SERS

Films created from noble metal nanostructures are of considerable current interest in nanotechnology due to the exceptional optical properties introduced by localized surface plasmon resonances (LSPRs). The excitation of LSPRs, which arises from the excitation of a collective electron oscillation within the metallic nanostructure induced by the incident light, leads to enormous optical local-field enhancement and a dramatic wavelength-selective photon scattering and localization at the nanoscale.[1−6] Much attention has been focused on ways of controlling the LSPR properties of metallic films, such as the position of resonant peaks, transmission pass-bands, and the magnitude of the optical-field enhancement, all of which are highly dependent on the size, shape, and composition of the metallic nanostructure as well as the refractive indices of the surrounding dielectric.[7−9] Recent research has shown that metallic nanostructure films with such unique optical properties have applications in biochemical sensing and imaging,[5−20] solar-cell design,[21−29] and optical processes,[30−33] as well as in many other fields.

Two typical potential applications of the biochemical sensing field using films constructed from metallic nanostructures are in the development of solid surface-enhanced Raman scattering (SERS) substrates and LSPR biosensors. SERS is an effective technique to enhance the specific Raman scattering spectrum of molecules in close proximity to a metal surface and is widely used for high-sensitivity molecular identification.[3] Experiments have shown that SERS enhancement factors of highly anisotropic metallic nanoplates or nanorods and aggregated nanoparticle clusters are much higher than those of spherical metallic nanoparticles. This occurs because the electromagnetic field at the sharp corners of these anisotropic nanostructures or in the gap region between clusters can be increased by several orders of magnitude, producing "hot spots" that are not present in isolated spherical nanoparticles.[1,10−14,34−41] As SERS spectra of molecules adsorbed on solid substrates are much more stable and repeatable compared with those in metal colloidal suspensions,[12,13] there is much interest in the development of solid SERS substrates having large Raman enhancements and good SERS reproducibility by using specific nanostructures incorporating hot spots.[10−20] LSPR biosensors operate by detecting real-time changes in the spectral position and magnitude of the LSPR due to local refractive index changes near metallic nanostructures.[3−7]

* Address correspondence to a2hu@uwaterloo.ca, tzhang@seu.edu.cn.

Received for review August 30, 2011 and accepted September 28, 2011.

Published online September 28, 2011
10.1021/nn203336m

A major concern in the practical implementation of LSPR biosensors is the development of a set of metallic nanostructured substrates with widely tunable LSPR wavelengths to achieve the highest sensitivity for various molecules with different refractive indices.[6]

Another application is the use of metallic nanostructure films to enhance the light trapping ability of solar cells.[21] Due to the LSPR effect, metallic nanostructures deposited on the surface of a photovoltaic device can serve as sub-wavelength scattering elements that efficiently trap incident sunlight and couples it into the photovoltaic absorption layer. This results in a significant improvement in the effective utilization of solar energy.[21−29] Previous experiments usually chose island-size or spherical metallic nanoparticles as the plasmonic scattering element,[22,23] but recent studies have suggested that the light-trapping performance of plasmonic scattering layers can be significantly improved by employing nonspherical, anisotropic metallic nanostrucutres with red-shifted and broadening LSPR (*e.g.*, nanoplates).[24,26] Thus, it is important to develop inexpensive, large-scale metallic nanostructure films having excellent scattering enhancement and widely tunable LSPR properties to maximize light trapping for spectral regions where it is most needed in solar cells.

Currently available methods for the fabrication of metallic nanostructure films include electron-beam lithography, which can completely control the formation and shape of the nanostructures for the design of metallic films with unique LSPR spectra but are too expensive for practical applications.[12−15] Other processes such as island annealing[16,23,24] or sintering[34,35] are low-cost and large-scale techniques but cannot control the shape of nanostructures. Mask-assisted deposition[27] and nanoimprintation[18,19,28,42] are also useful in the construction of regular nanostructure arrays using metallic strips or nanospheres, but it is difficult to create elemental components with a gap distance of a few nanometers as occurs in multimer aggregates. A completely different inexpensive, mask-less method consists of the self-assembly of colloidal particles to produce large-area metallic films involving shaped metallic nanoparticles. This technique has promise in practical applications in biosensing and photovoltaics.[20,22,43−46] However, currently self-assembled metallic films are usually fabricated in an organic-solvent environment[10,43] or by using surface-modified substrates after complex modification processes.[20,44−46] It is still a challenge to assemble large-scale colloidal metallic particles on unmodified glass, or directly on organic substrates,[46] especially in aqueous solution.

From this discussion, it is obvious that a primary challenge in creating large-scale plasmonic films is the development of fabrication techniques that are simple and straightforward, less substrate-dependent, and effective in controlling and engineering LSPR spectra. In this paper, we describe a simple self-assembly method using silver nanoplates (SNPs) to fabricate reproducible, large-area ultrathin metallic films suitable for unmodified substrates made from different materials. These films have widely tunable LSPR properties combined with enormous scattering enhancement. We find that, compared to conventional self-assembled spherical metallic nanoparticles, metallic films constructed using size-controllable SNPs exhibit a much wider frequency-selective response that extends from visible to near-infrared wavelengths and has a much better refractive-index sensitivity to surrounding dielectrics. In addition we find that the bandwidth (fwhm) and the resonance peak position of the plasmon resonance spectrum of the metallic films can be engineered by controlling SNP aggregation. A three-dimensional (3D) finite element method (FEM) simulation was employed to give an in-depth explanation of these specific LSPR properties of these metallic film samples. The scattering of the SNP films with different particle number density was exhibited and evaluated quantitively using prism coupling. Finally, we demonstrate the excellent scattering enhancement ability of these metallic films by using them as substrates in SERS measurements and find that SERS spectra are increased by several orders of magnitude over those obtained from metallic films assembled using typical spherical silver nanoparticles.

RESULTS AND DISCUSSION

In the first step, we synthesized size -selected colloidal dispersions of SNP according to previously reported chemical synthetic methods[47] with a modified material concentration. This represents a rapid approach to the fabrication of high-concentration samples of colloidal SNP at room temperature. We chose SNP because previous studies have established that the scattering enhancement and the tunability of the LSPR peak position of such nanoparticles due to their anisotropic geometry are much better than that of spherical nanoparticles.[47−51] In addition, compared with silver nanorods, which always show multi-LSPR peaks,[41] SNPs are better candidates for the development of films with tunable spectral response because they show a nearly single LSPR peak corresponding to the longitudal resonance in the LSPR spectra of SNPs.[48,49] SNP colloids were first centrifuged and then redispersed in deionized water. Evolution of the shape of SNPs in colloids is shown in Figure S1. Polyvinylpyrolidone (PVP) and ascorbic acid were then added into the solutions in sequence under strong stirring. Single-layer self-assembled SNP films can be obtained by immersing the substrates with hydrophobic surfaces into the SNP solution under controlled conditions.

In this experiment, ascorbic acid has been found to be a key ingredient for the self-assembly production of large-scale silver films in aqueous solution because it can modify the surface activity of SNPs significantly. (A comparison of the self-assembled film in silver colloids with different chemical ingredients can be found in Figure S2.) Before ascorbic acid was added, a small amount of PVP was added into the solution. PVP is usually used as a shape-directing agent or stabilizer during the synthesis procedures of shaped silver nanoparticles.[8,41,50] In our case, PVP has been found to keep anisotropic nanoplates stable and well-dispersed, inhibiting agglomeration. Figure 1 shows a comparison of TEM images of typical colloidal dispersions after adding different chemical ingredients.

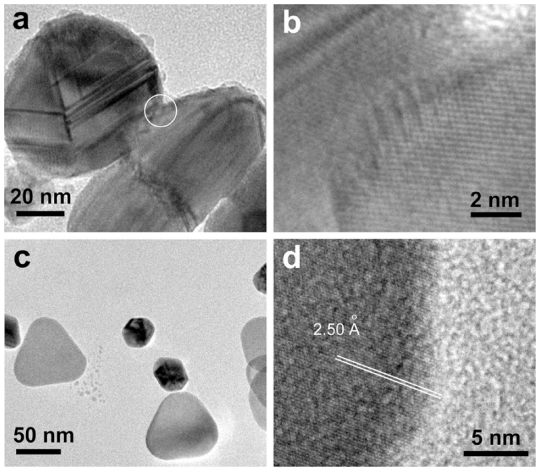

Figure 1. TEM images of (a) purified silver colloids by adding ascorbic acid and (c) purified silver colloids by adding PVP and ascorbic acid in sequence. (b) HRTEM image at the junction of the nanoparticles labeled in (a). (d) HRTEM image at the edge of the SNP in (c).

Figure 1a shows that, without the stabilization of PVP, the shape of the SNP changes significantly and the nanoparticles readily coalesce in the presence of ascorbic acid. The high-resolution transmission electron microscopy (HRTEM) in Figure 1b clearly shows this coalescence between two silver nanoparticles and indicates that they are polycrystalline at their junction. Figure 1c and d show low- and high-magnification TEM images of purified silver colloids by adding PVP and ascorbic acid in sequence. From Figure 1c one can see the colloids contain well-separated triangular nanoplates with blunted corners. The HRTEM image in Figure 1d shows that SNPs are single crystals with the 2.50 Å spacing between lattice fringes. The thickness of the SNP is between 8 and 20 nm, which is dependent on the amount of silver seeds added during the colloid synthesis (Figure S1, Supporting Information).

A picture of a typical self-assembled SNP film on a glass substrate and its corresponding scanning electron microscope (SEM) image on a silicon wafer (inset) are shown in Figure 2a. Figure 2b shows a picture of a SNP film on a flexible polyethylene terephthalate substrate. The straightforward self-assembly on unmodified substrates made from different materials makes this method useful for various practical applications. By adding different amounts of silver seeds during the colloid synthesis procedure, samples a–f of colloidal SNP with different particle sizes were prepared and then deposited onto uniform silver films on glass microscope slides as shown in Figure 2c–e. We focused our study on SNP films on glass microscope slides because the glass substrate is optically transparent over a wide wavelength range and has a smooth optical surface with high chemical stability. Therefore measurements of the LSPR properties of SNP films may not be confused by the

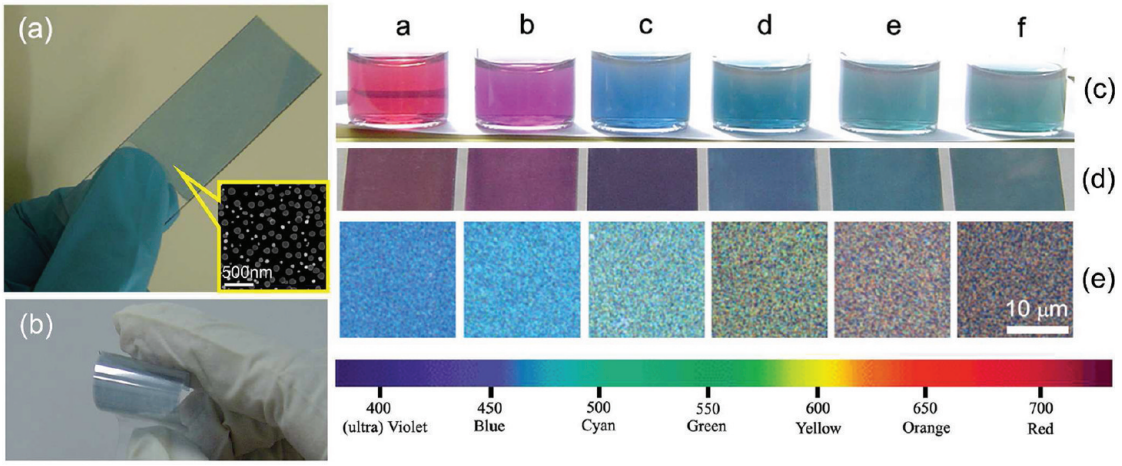

Figure 2. (a) Typical silver nanostructure film on a glass substrate and its corresponding SEM image on a silicon wafer (inset). (b) Silver nanostructure film on a flexible polymeric substrate. (c, d) Photographs of a series of samples of the diluted silver colloids and the corresponding silver film consisting of SNPs having different particle sizes. (e) Corresponding optical microscopic images of the SNP films under white light illumination. The particle sizes of samples a–f were dependent on the concentration of the silver seeds in the synthesis procedures. Note that the dark blue color that can be found in all of the six samples in (e) is intrinsically the background color in the optical microscopy and is not the color of the nanoparticles. The average size of SNPs corresponding to samples a–f taken from SEM images is 50, 57, 78, 96, 142, and 158 nm, respectively.

optical spectral properties of the substrate. However, the design constraints described here can be easily extended to a wide range of different substrate materials. Significant changes in the colors of the silver colloids (Figure 2c) and films (Figure 2d) were observed due to the selective optical absorption and scattering behavior of SNP with specific particle sizes. Photographs (Figure 2c, d) show that sample color changes from red to purple, mauve, blue, and green as the SNP particle size increases. More interesting is the color evolution shown in Figure 2e. The color in the corresponding optical microscopic images (bright-field, white light illumination) of these silver films changes from blue to cyan, green, yellow, orange, and red following the evolution of the visible spectrum, as illustrated at the bottom of Figure 2. The distinct color changes between the photographs (shown in Figure 2c and d) and the optical microscopic images (shown in Figure 2e) of the films arise from different optical phenomena induced by the SNPs. The color of the samples exhibited in the photographs is intrinsically a "color mixing" effect resulting from the selective optical absorption associated with the reflection of natural light arising from the plasmon resonance of SNP. This contrasts with the color of silver films seen in optical microscopy, which are mainly produced by the strong electromagnetic backward scattering enhancement and the localization of SNP at certain wavelengths. As illustrated in Figure 2e, the continuous color change from short to long wavelength indicates that these silver films are uniform over a large area and have high enhancement of their wavelength-dependent scattering properties.

Tunable Peak Position of the LSPR. To study the plasmon resonance characteristics of monolayer SNP films, extinction and diffuse reflectance spectra of the silver films were measured. Figure 3a and b show a comparison between the normalized extinction spectra of silver colloids and those of the corresponding silver films, respectively. Extinction spectra of all the as-prepared SNP films display two resonance peaks. The main resonance peak at long wavelength is attributed to the in-plane dipole resonance of SNP, while the second peak at about 410 nm is attributed to spherical silver nanoparticles (Figure 1c), together with the out-of-plane dipole resonance of SNP.[48] It has been found that using the current self-assembly method the LSPR peak position of the SNP film can be fine-tuned from visible wavelengths to the near-infrared by simply using SNPs having different sizes. Slight increases in amplitude at longer wavelength can be observed in the extinction spectra (Figure 3b) and can be attributed to the aggregation of SNP as discussed in the next section. Normalized diffuse reflectance spectra of the silver films in Figure 3c show the excellent wavelength-selective scattering enhancement ability of SNP films over a broad spectrum, especially at long wavelengths. These findings indicate that incident long-wavelength

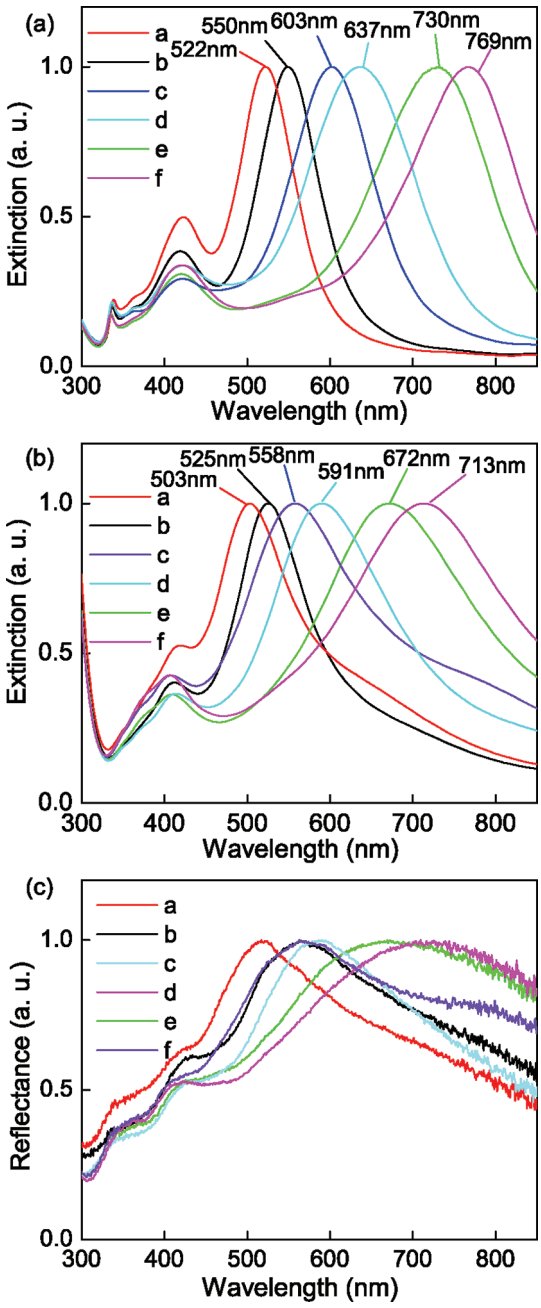

Figure 3. (a) Normalized extinction spectra of the silver colloids. (b and c) Normalized extinction spectra and diffuse reflectance spectra, respectively, of silver films. The labels a to f represent samples a–f.

radiation can be strongly localized and reflected back at the surface of anisotropic SNP films and the central resonance wavelength can be easily tuned by using SNPs with different particle sizes. This is a primary advantage for these SNP films because the LSPRs of conventional silver films consisting of silver nanospheres or nanoholes are not easily tuned to long wavelengths. Figure 3b and c also demonstrate that both the absorption and the scattering behaviors of plasmonic nanoparticles can be significantly enhanced near LSPR wavelengths.

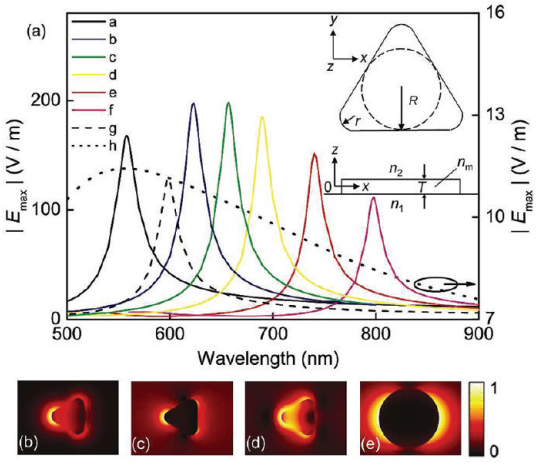

Figure 4. (a) Refractive-index-dependent LSPR spectra for an individual silver nanosphere or SNP surrounded by different dielectrics. Curves a−f represent the LSPR spectra for an individual SNP placed on the surface of a glass slide (n_1 = 1.52) and covered with dielectrics having n_2 = 1.0, 1.33, 1.48, 1.61, 1.8, and 2, respectively. Curve g represents the LSPR spectrum for an individual SNP immersed in water ($n_1 = n_2$ = 1.33). In the simulation, the structural parameters of the SNP are set as R = 22 nm, r = 11 nm, and T = 16 nm. Curve h represents the LSPR spectrum for an individual silver sphere with a radius of 75 nm on a glass substrate and covered by air (n_2 = 1) in which the fwhm is as broad as ~250 nm. (b−d) Cross-sectional views (z = 0) of the normalized electric-field $|E|$ distribution of the SNP with n_1 = 1.52 and n_2 = 1 at λ = 558, 900, and 500 nm, respectively. (e) Cross-sectional view of the $|E|$ distribution at the center of a silver nanosphere having a radius of 75 nm, n_1 = 1.52, and n_2 = 1 at λ = 560 nm.

The high refractive-index sensitivity of SNP can also been seen by comparing extinction spectra of silver colloids with those of silver films. A noticeable blue-shift of the long-wavelength peak was observed for all silver films compared to that of the silver colloids. Referring to the second plasmon resonance peak at ~410 nm corresponding to the silver nanospheres, the shift of the resonance peak is more obvious for the anisotropic SNP, especially for those with large particle sizes. We illustrate the refractive index sensitivity of SNP in Figure 4 using 3D-FEM simulations generated with the numerical program package COMSOL Multiphysics, which has been found to be an effective tool for the modeling of plasmonic devices.[52,53] A rectangular wave with a transverse magnetic (TM) 01 mode is used as the incident light. The geometry of our model from the top (x−y plane) and from the side (x−z plane) is shown in the inset of Figure 4a, respectively. For accurate agreement with the experimental sample, we define the values of three structural parameters: the inner radius of the nanoplate, R = 22 nm, the corner radius, r = 11 nm, and the thickness, T = 16 nm. The nanoplate is placed on the surface of a substrate refractive index n_1 and covered with a dielectric layer having a refractive index n_2. The complex refractive index of silver, n_m, is fitted analytically using experimental data.[54] Figure 4a shows refractive-index-dependent LSPR spectra as a function of the wavelength λ for an individual silver nanosphere or SNP surrounded by different dielectrics. First, the comparison of the LSPR spectra in curve a (n_1 = 1.52, n_2 = 1) and curve g ($n_1 = n_2$ = 1.33) shows a noticeable blue-shift from 598 nm to 558 nm, corresponding to placing the nanoplate on a glass substrate instead of having it in water. Both the resonance peak position and the predicted blue-shift in the simulation are in good agreement with the results of our experiments (sample c in Figure 3a and b), establishing the high accuracy of the 3D model. In a further test to evaluate the refractive-index sensitivity of SNP films, the plasmon resonance for a nanoplate with fixed n_1 and different values of n_2 has been simulated. Curves a−f represent LSPR spectra for an individual SNP placed on the surface of a glass slide (n_1 = 1.52) and covered by different dielectrics with n_2 = 1.0, 1.33, 1.48, 1.61, 1.8, and 2. A significant red-shift from visible to near-infrared wavelengths is observed as n_2 increases. The LSPR wavelength change per refractive index unit (RIU) is 240 nm/RIU (Figure S3, Supporting Information), which is much higher than that of previously reported gold island substrates (66−153 nm/RIU) and silver nanospheres (110 nm/RIU).[16,25] Compared with the simulation of spherical silver nanopartices,[25] it is clear that the LSPR peak in the SNP film is much more sensitive to refractive-index changes in the dielectric overlayer and maintains a sharp resonance band even when the peak position moves into the near-infrared. We also found that the amplitude of the plasmon peak is over 100 times larger and the fwhm is only about one-eighth for a SNP (curve a) compared to that of a silver nanophere (curve h). Comparing the cross-sectional view (z = 0) of the normalized electric-field $|E|$ distribution in a SNP and a silver nanophere (Figure 4b−e) shows that the enormous LSPR of SNP films can be attributed to the anisotropic geometry of nanoplates, which leads to a significant electric-field enhancement in the vicinity of the sharp corner area at the resonance wavelength (Figure 4b). This electromagnetic localization effect in the SNP is strongly wavelength-dependent and becomes much weaker when the incident light deviates from the resonance wavelength as shown in Figure 4b and c. At longer wavelengths (Figure 4c) the electromagnetic localization behavior at the corners of the nanoplate becomes less apparent. By comparison, at short wavelength (Figure 4d) a large fraction of the light can penetrate deep into the nanoplate without significant attenuation. This unique property enables SNP to serve as a narrow waveband antenna with strong wavelength selectivity.

Tunable Bandwidth of the LSPR. LSPR bandwidth tunability in SNP films is also of much interest in addition to the tunability of the peak position in these materials. We fabricated three silver films with different LSPR spectra using the following processes: 24 mL of centrifuged

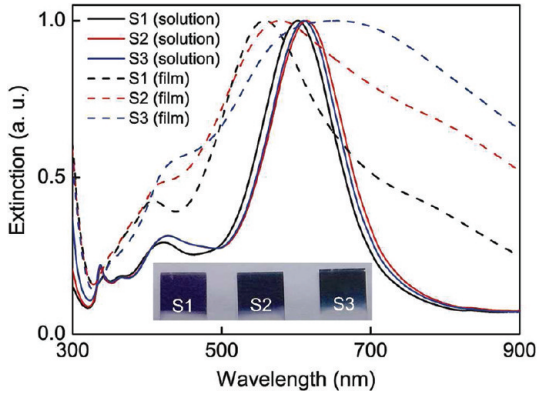

Figure 5. Extinction spectra of SNP colloids (solid lines) and films (dashed lines) for samples S1−S3. The inset shows photographs of the samples.

colloid containing SNPs with PVP shells (sample c) was divided into three equal parts, and then different amounts of ascorbic acid were added into the divided colloids. Three samples, S1, S2, and S3, were prepared with 0.1, 0.5, and 2 mL of 100 mM ascorbic acid, respectively. Finally, cleaned glass slides were immersed in these samples for approximately 20 h to achieve self-assembled SNP films. This fabrication processes ensured that the elemental components of the silver films are SNP having the same average particle size. Figure 5 shows the extinction spectra of SNP colloids and films for samples S1, S2, and S3. The photographs of the samples are shown in the inset. As there are only slight differences in these spectra of SNP colloids, it is reasonable to assume that the LSPR properties of SNP are similar in the suspended state despite the addition of different amounts of ascorbic acid. However, major changes in these extinction spectra occur when SNP films from the three samples are deposited on glass slides. With an increase in the amount of ascorbic acid, the LSPR peak position shows a red shift from 598 to 680 nm and the fwhm of the resonance band is broadened significantly. This finding indicates that the localization and the absorption enhancement of the SNP film at longer wavelengths were greatly improved by the addition of ascorbic acid. Images of the three SNP films in the inset of Figure 5 showing a color change from violet to blue and finally to green confirm this difference in the LSPR property. SEM images of the particle distribution in these films (Figure 6a and b) compare the morphologies of the SNP films corresponding to samples S1 and S3, respectively. It can be seen that these two films consist of monolayer SNPs together with a small quantity of silver nanospheres and are uniform over a large area. It is interesting that the particle sizes of the SNPs in the two films are almost the same (Figure S4a, Supporting Information); however, the particle number density in the two films is quite different. Higher magnification SEM images (inset of Figure 6a and b) clearly show this

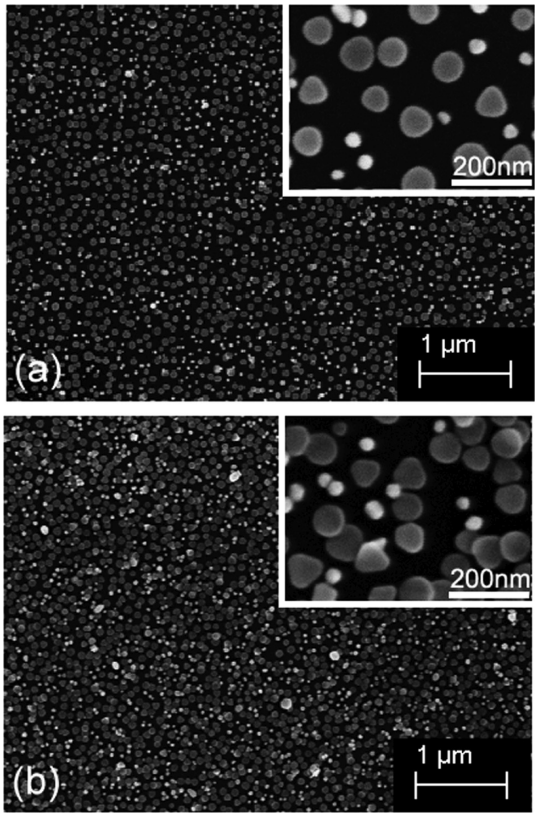

Figure 6. (a, b) Comparison of the top-view SEM images of the SNP films corresponding to samples S1 and S3, respectively. Insets in (a) and (b) correspond to higher magnification SEM images for samples S1 and S3, respectively.

difference in particle distribution (details are shown in Figure S4b, Supporting Information). In sample S1, the distances between the SNPs are relatively large (~30−200 nm), and only a few dimers and trimers can be observed. Seventy percent of the SNPs are isolated. With this type of distribution, the optical spectral properties of the silver film are mainly decided by the LSPR of individual SNPs. This explains why the extinction spectrum of sample S1 is well matched with the simulated LSPR spectrum of an individual SNP (curve a in Figure 4a). For sample S3, it is apparent that the particle number density of the film is much higher compared to that of S1. Only 29% of the SNPs are isolated. From the inset in Figure 4b one can see that the SNPs are in close proximity and are accompanied by a variety of SNP dimers, trimers, and long nanochains having different configurations randomly distributed on the surface of the film. As shown previously, the LSPR property including the scattering enhancement and the resonance peak position for aggregated spherical or polyhedral metallic nanoparticles is different from that of a separated nanoparticle owing to a strong plasmon coupling effect.[1,38−40] Here we show that there are two primary factors leading to significant changes of the LSPR properties for silver films formed from aggregated anisotropic SNPs. The first factor is the gap distance between the SNPs. Using 3D-FEM,

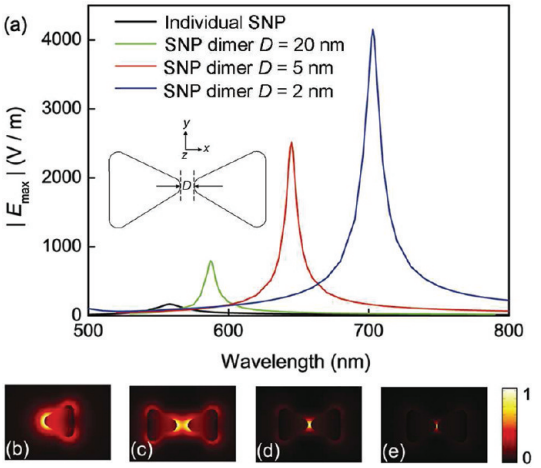

Figure 7. (a) LSPR spectra for SNP dimers with different gap distances *D* placed on the surface of a glass slide (n_1 = 1.52) and covered with air (n_2 = 1.0). The inset illustrates the geometry of our simulation model in the *x*−*y* plane (*z* = 0). (b) Normalized electric-field distribution at a resonance at the center of an individual SNP. (c−e) Comparison of the normalized electric-field distribution at the center of the SNP dimer with *D* = 20, 5, and 2 nm, respectively.

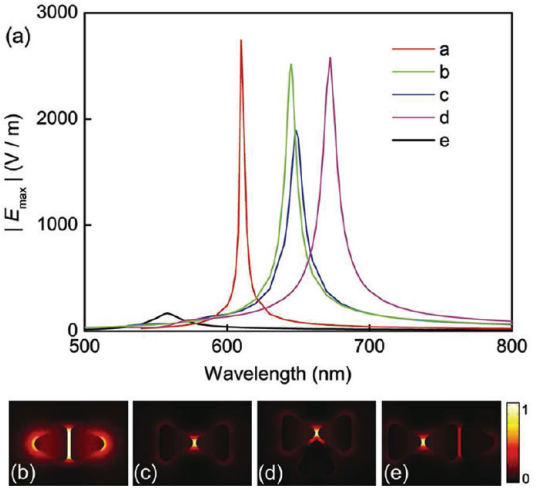

Figure 8. (a) LSPR spectra for SNP dimers and trimers with different morphological structures placed on the surface of a glass slide (n_1 = 1.52) and covered with air (n_2 = 1.0). The gap distance between the SNP was set at 5 nm. The normalized electric-field distributions at the resonance wavelength within curves a−d can be found in (b−e), respectively. Curve e represents the LSPR spectrum for an isolated SNP.

we have simulated the LSPR spectra (Figure 7a) for a silver nanoplate dimer with different gap distances *D* placed on the surface of a glass slide (n_1 = 1.52) and covered by air (n_2 = 1.0) having the geometry in the *x*−*y* plane as illustrated in the inset of Figure 7a. The structural parameters for an individual SNP are the same as described in Figure 4. A dramatic resonance enhancement along with an obvious red-shift of the resonance peak from 580 to 720 nm can be observed when the value of *D* decreases from 20 to 2 nm. It can be seen that the maximum amplitude of the normalized electric field $|E_{max}|$ for a SNP dimer with *D* = 2 nm is approximate 25 times greater and 200 times greater than that of a separated SNP and a silver nanosphere (Figure 4a), respectively. Normalized electric-field distributions at the resonance wavelengths of SNPs having different geometries are shown in Figure 7b−e. The electromagnetic-field distributions indicate that the incident light at the LSPR wavelength can be strongly localized in the ultrasmall volume between the two SNPs due to the strong plasmon coupling effect. This simulation confirms that particle number density is one of the primary factors in determining the red-shift of the peak position and the broadening of the resonance band in the extinction spectra of S2 and S3. In addition to the gap distance, the characteristics of the LSPR in the silver film are influenced by the presence of silver dimers, trimers, or larger aggregates randomly distributed in the monolayer film (inset of Figure 6b). Figure 8a shows LSPR spectra for typical silver dimers and trimers with the morphologies given in Figure 8b−e. The structural parameters for the elemental SNPs are the same as above. The minimum gap distance *D* between these aggregated SNPs is set at 5 nm. It can be seen that the LSPR peak position also depends on the morphology of the adjacent SNPs. Compared to that of individual SNPs, the LSPR peak positions in silver dimers and trimers shift to between 600 and 700 nm. From Figure 8d and e one can see that the electric-field distributions are asymmetrical and are enhanced in the vicinity of corners. Figure 8d shows that although there are three corners with a similar gap distance in the silver trimer, the enhancement in the electromagnetic field occurs only at the in-plane corner. This localized electromagnetic enhancement can be attributed to the nature of the polarization dependence of plasmonic structures as discussed previously.[30] It also appears that the LSPR peak is longer for the long chain structure (curve d corresponding to the morphology in Figure 8e). It is significant that the LSPR peak moves to longer wavelength when more SNPs are tightly packed.

The simulations in Figures 7 and 8 indicate that the red-shift and the broadening of the LSPR spectra for samples S2 and S3 are induced by the aggregation of the SNPs. This implies that, by the addition of optimized amounts of ascorbic acid in the present self-assembly method, it is straightforward to fabricate SNP films with controlled LSPR bandwidth and peak position. These samples also contain a large number of randomly distributed hot spots having significantly enhanced scattering and light-trapping properties at long wavelengths. This property can be regarded as one of the primary advantages of the present self-assembly method, which may be very useful in biosensing and photovoltaics applications. For example, the extinction spectrum of sample S2 in Figure 5 is well matched with the AM 1.5 solar spectrum.[21] By incorporating a thin layer of SNP film into solar cell devices,

light trapping and scattering of the solar cell can then be improved significantly over a wide range, especially at long wavelengths.

Furthermore, as shown in the SEM images in Figure 6, the films with different particle number densities maintain a monolayer in large scale during the deposition process. Such monolayer morphologic deposition is generated by a self-organization of SNPs combined with the optimization of the concentration of ascorbic acid and the deposition time. This ensures that the SNP films are ultrathin (8−20 nm) compared to most metallic films consisting of other types of nanoparticles.

Quantitive Analysis of Scattering Enhancement. To quantitively analyze the scattering enhancement effect from SNP films self-assembled on glass substrates, we have measured the scattered light from the SNP film using a prism coupler together with a charge-coupled device (CCD) camera (see Figure S5, Supporting Information). This method has been used to monitor the scattered signal at the surface of an optical waveguide in our previous experiments.[55] The laser beam was coupled into the glass substrate by prism coupling from the right side of the glass slide, which is not coated with an SNP film. With certain incident angles, the obliquely incident laser beam can reflect between the upper and lower surface of the glass slide and propagate forward in a zigzag pattern. The scattered light signal is significantly enhanced when the laser beam reflects through the SNP film deposited on the surface of the glass substrate. In this experiment, a TM mode laser beam with a wavelength of 632.8 nm, which is near the LSPR peak of samples S1−S3, was used as the incident light source. A CCD camera was used to monitor the intensity of the scattered light along the propagation path looking from the top. Figure 9 shows the intensity of the scattered light along the propagation light path for S1−S3. The dashed line at position = 0 corresponds to the edge of the SNP film. Peaks separated by a constant amount in these curves correspond to scattering points at the surface between the glass substrate and air. The amplitude of the peaks of the scattered light is weak when light is reflected at the smooth surface of the glass substrate without SNP films (position > 0). When the light beam passes through the glass substrate with SNP films on the surface (position < 0), it is clear that the scattered light signal increases significantly as a result of the plasmon resonance of SNPs. The first scattering peak at the left side of the dashed line shows the amplitude of the intensity of the scattered signal is enhanced by 5, 8, and 17 times for S1−S3, respectively. This experimental result confirms our theoretical simulation as discussed previously. When SNPs are in close proximity (S3), the intensity of the scattered light is strongly enhanced due to the coupled plasmon resonance corresponding to hot spots. A comparison of photographs of the propagation light path for S1 and S3 in the inset of Figure 9

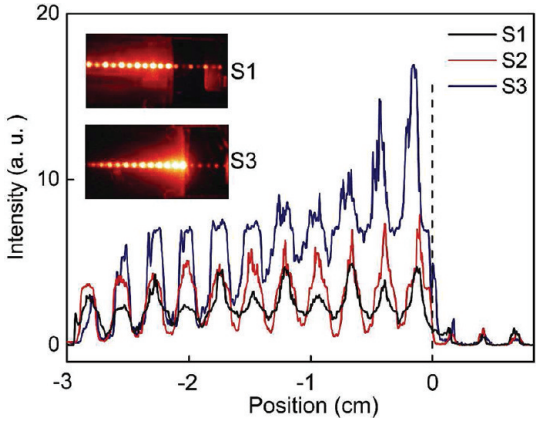

Figure 9. Comparison of the scattered light intensity for samples S1−S3. Insets show photographs of the scattering images for samples S1 and S3, respectively.

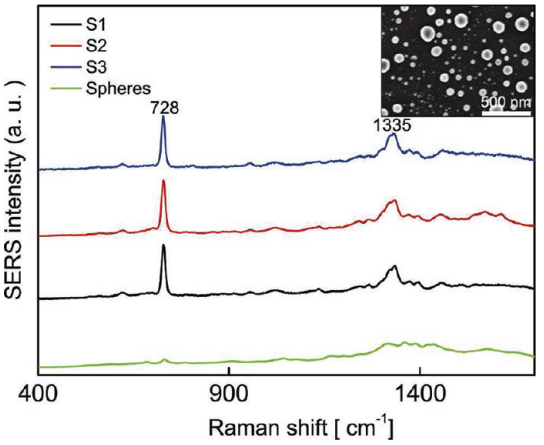

Figure 10. SERS spectra of adenine molecules with a concentration of 10^{-4} M obtained from the films of samples S1−S3 and a film formed by large spherical silver nanoparticles. The inset shows the SEM image of the film containing large spherical silver nanoparticles.

clearly shows high scattering enhancement of the SNP films. We also observed that the intensity decreases rapidly along the propagation path for S3 in Figure 9 because more light is scattered from the surface of the glass substrate. Diffuse reflectance spectra (Figure 3c) and the scattered light intensity measurement in Figure 9 experimentally demonstrate the excellent backward and forward scattering enhancement properties of the SNP films, respectively. Therefore, such SNP films may be used to significantly improve the light-trapping and scattering properties of solar cells and biosensors.

SERS Activity Investigation. To investigate the performance for electromagnetic enhancement and the biocompatibility of the SNP films, SERS spectroscopic measurements were carried out using adenine, a well-characterized test molecule. Spectra obtained of adenine molecules at a concentration of 10^{-4} M are shown in Figure 10. All the samples S1−S3 exhibited repeatable high SERS sensitivity because the characteristic Raman peak in adenine molecules at 728 cm^{-1} is quite

sharp, in agreement with previous results.[56] By comparison with the SERS spectrum obtained using a silver film formed using spherical silver nanoparticles as a substrate (inset of Figure 10), the SERS signal of molecules adsorbed on the surface of a SNP film substrate is several orders of magnitude stronger. This further supports our finding that the electromagnetic enhancement in anisotropic SNP and the aggregated SNP multimers is much greater than that occurring with spherical silver nanoparticles. In this experiment, however, we did not observe any obvious difference between SERS spectra obtained from samples S1–S3. We suspect that this is because both anisotropic SNP (in sample S1) and the aggregated multimers (in samples S2 and S3) are both effective in providing a large number of hot spots for SERS enhancement.

CONCLUSIONS

We report a robust self-assembly method suitable for the fabrication of large-scale, ultrathin, monolayer metallic films on the surface of a variety of unmodified substrates. Compared with previously reported self-assembly methods, the present technique is simpler, faster, and low-cost, as it can be carried out in aqueous solution at room temperature without evaporation of a solvent or sample heating. Because SNPs can have an anisotropic structure, the LSPR peak position of the monolayer films can be finely tuned over a wide spectral range extending from visible to near-infrared wavelengths. Resonances with reproducible fwhm and significantly enhanced light trapping and scattering properties can be obtained by simply changing the sizes and the gap distances of the SNPs. Combining experimental and theoretical studies, we find that the present metallic films have a high refractive-index sensitivity and significant scattering enhancement. In addition, the tunability of the LSPR peak position makes these SNP films promising materials for the development of highly sensitive SERS-active substrates for molecular identification and LSPR biosensors sensitive to the refractive indices of surface-bonded species. Controllable aggregation of the SNPs also leads to an extended fwhm of the LSPR band associated with significant enhancement of scattering and light-trapping properties at long wavelengths. By proper engineering of LSPR properties, these monolayer SNP films could be integrated into thin-film solar photovoltaic devices resulting in a dramatic improvement of the trapping performance of the absorber layer in the full solar spectrum, especially in the visible and near-infrared ranges. This unique combination of properties implies that these SNP films have great potential utility in fields as diverse as optical displays, color filtering, and optical processing.

METHODS

Preparation of Silver Seeds. A 0.5 mL amount of 59 mM $AgNO_3$ and 1 mL of 34 mM trisodium citrate were added to 10 mL of deionized water (>18.4 MΩ·cm). Then 0.5 mL of 20 mM $NaBH_4$ was added. The resultant solution was stirred for 20 min and aged for at least 24 h at room temperature before use.

Preparation of Solutions 1 and 2. Solution 1: 50 μL of aqueous 400 mM hydrated hydrazine, 60 μL of aqueous 400 mM trisodium citrate, and different quantities of silver seeds were added to 20 mL of deionized water. Solution 2: 60 μL of 590 mM $AgNO_3$ was added to 6 mL of deionized water.

Synthesis of SNP Colloids. Solution 2 was added dropwise (1 mL/min) into solution 1 under strong stirring conditions. As a result, colloidal dispersions containing SNP can be achieved. Six samples, a–f, were prepared in which the quantity of silver seeds added in solution 1 was 210, 160, 80, 70, 50, and 40 μL, respectively. These colloidal dispersions were purified using centrifugation to reduce the abundance of nanospheres, which are a common byproduct of the synthesis. Typically, 60 mL of freshly prepared SNP colloidal dispersions was centrifuged at a low speed (2000–4000 rpm, dependent on the sizes of the SNPs) for 45 min to sediment SNPs. After removing the yellow supernatant, which contains mainly the small spherical nanoparticles, the sediment was redispersed with 20 mL of deionized water. Figure S1 indicates that the concentration of silver nanospheres decreases after centrifuging. The proportion of nanospheres remaining is between 20% and 45% as estimated from SEM images. It should be noted that the remaining nanospheres showed very limited influence on the LSPR spectra of the SNP films because only less than 10% of the area of the substrate was covered by these nanospheres. This is shown in Figure 6.

Preparation of Metallic Nanostructured Films. After purification, PVP and ascorbic acid were then added into the purified SNP solutions in sequence under strong stirring. Typically, 10 mL of 2 mM PVP was added in 25 mL of silver colloid under strong stirring for more than 10 min, and then 0.3 mL of 100 mM ascorbic acid was added. Glass slides, silicon wafers, or polymeric substrates with hydrophobic surfaces were cleaned using detergent and deionized water in sequence and then dried. The cleaned substrates, without any need for further surface modification, were immersed vertically into the colloids for approximately 20 h. Single-layer SNPs then uniformly self-assembled on the surfaces of the substrates.

Measurements. TEM and HRTEM observations were performed using a FEI Tecnai 20 operating at 200 kV (point resolution 2.4 Å, line resolution 1.44 Å). SEM images were obtained using a field-emission SEM (Leo1530 Zeiss, Germany). Optical microscopic images were taken using an Olympus BX51 M System metallurgical microscope (100 × 0.80). Extinction spectra and diffuse reflectance spectra of the silver colloids and the films were obtained using a UV–vis spectrophotometer (UV-2501 PC, Mandel Shimadzu). A prism coupler (SPA4000, Korea) and a CCD camera (Canon EOS 5D) were used for the measurement of the scattering enhancement of the SNP film. SERS spectra were obtained using a Renishaw micro-Raman spectrometer with an objective magnification of 50× and an excitation wavelength of 488 nm.

Acknowledgment. This work is supported by NSFC under grant no. 60977038, NSFC-Research Fund for International Young Scientists under grant no. 60910187, the National Basic Research Program of China (973 Program) under grant no. 2011CB302004, the Scientific Research Foundation of Graduate School of Southeast University under grant no. YBJJ0925, Graduate Innovation Program of Jiangsu Province under grant no. CX09B_050Z and CXLX_0114, and the Foundation of Key Laboratory of Micro-Inertial Instrument and Advanced Navigation Technology, Ministry of Education, China, under grant nos. 201012 and 201005. This work is partially supported by NSERC

discovery grants and Canada Research Chairs program on microjoining, Canada.

Supporting Information Available: More details about the particle distribution in the SNP colloids and SNP films, additional experiment relating to the self-assembling, and a scheme of the scattering light measurement are provided. This material is available free of charge *via* the Internet at http://pubs.acs.org.

REFERENCES AND NOTES

1. Halas, N. J.; Lal, S.; Chang, W. S.; Link, S.; Nordlander, P. Plasmons in Strongly Coupled Metallic Nanostructures. *Chem. Rev.* **2011**, *111*, 3913–3961.
2. Lu, X. M.; Rycenga, M.; Skrabalak, S. E.; Wiley, B.; Xia, Y. N. Chemical Synthesis of Novel Plasmonic Nanoparticles. *Annu. Rev. Phys. Chem.* **2009**, *60*, 167–192.
3. Willets, K. A.; Van Duyne, R. P. Localized Surface Plasmon Resonance Spectroscopy and Sensing. *Annu. Rev. Phys. Chem.* **2007**, *58*, 267–297.
4. Stewart, M. E.; Anderton, C. R.; Thompson, L. B.; Maria, J.; Gray, S. K.; Rogers, J. A.; Nuzzo, R. G. Nanostructured Plasmonic Sensors. *Chem. Rev.* **2008**, *108*, 494–521.
5. Yonzon, C. R.; Stuart, D. A.; Zhang, X. Y.; McFarland, A. D.; Haynes, C. L.; Van Duyne, R. P. Towards Advanced Chemical and Biological Nanosensors—An Overview. *Talanta* **2005**, *67*, 438–448.
6. Gao, S. Y.; Koshizaki, N.; Tokuhisa, H.; Koyama, E.; Sasaki, T.; Kim, J. K.; Ryu, J.; Kim, D. S.; Shimizu, Y. Highly Stable Au Nanoparticles with Tunable Spacing and Their Potential Application in Surface Plasmon Resonance Biosensors. *Adv. Funct. Mater.* **2010**, *20*, 78–86.
7. Mock, J. J.; Smith, D. R.; Schultz, S. Local Refractive Index Dependence of Plasmon Resonance Spectra from Individual Nanoparticles. *Nano Lett.* **2003**, *3*, 485–491.
8. Mulvihill, M. J.; Ling, X. Y.; Henzie, J.; Yang, P. D. Anisotropic Etching of Silver Nanoparticles for Plasmonic Structures Capable of Single-Particle SERS. *J. Am. Chem. Soc.* **2010**, *132*, 268–274.
9. Lu, L.; Kobayashi, A.; Tawa, K.; Ozaki, Y. Silver Nanoplates with Special Shapes: Controlled Synthesis and Their Surface Plasmon Resonance and Surface-Enhanced Raman Scattering Properties. *Chem. Mater.* **2006**, *18*, 4894–4901.
10. Speed, J. D.; Johnson, R. P.; Hugall, J. T.; Lal, N. N.; Bartlett, P. N.; Baumberg, J. J.; Russell, A. E. SERS from Molecules Bridging the Gap of Particle-in-Cavity Structures. *Chem. Commun.* **2011**, *47*, 6335–6337.
11. Le, F.; Brandl, D. W.; Urzhumov, Y. A.; Wang, H.; Kundu, J.; Halas, N. J.; Aizpurua, J.; Nordlander, P. Metallic Nanoparticle Arrays: A Common Substrate for Both Surface-Enhanced Raman Scattering and Surface-Enhanced Infrared Absorption. *ACS Nano* **2008**, *2*, 707–718.
12. Gopinath, A.; Boriskina, S. V.; Premasiri, W. R.; Ziegler, L.; Reinhard, B. M.; Dal Negro, L. Plasmonic Nanogalaxies: Multiscale Aperiodic Arrays for Surface-Enhanced Raman Sensing. *Nano Lett.* **2009**, *9*, 3922–3929.
13. Wang, S.; Pile, D. F. P.; Sun, C.; Zhang, X. Nanopin Plasmonic Resonator Array and Its Optical Properties. *Nano Lett.* **2007**, *7*, 1076–1080.
14. Chu, Y. Z.; Banaee, M. G.; Crozier, K. B. Double-Resonance Plasmon Substrates for Surface-Enhanced Raman Scattering with Enhancement at Excitation and Stokes Frequencies. *ACS Nano* **2010**, *4*, 2804–2810.
15. Berkovitch, N.; Ginzburg, P.; Orenstein, M. Concave Plasmonic Particles: Broad-Band Geometrical Tunability in the Near-Infrared. *Nano Lett.* **2010**, *10*, 1405–1408.
16. Karakouz, T.; Holder, D.; Goomanovsky, M.; Vaskevich, A.; Rubinstein, I. Morphology and Refractive Index Sensitivity of Gold Island Films. *Chem. Mater.* **2009**, *21*, 5875–5885.
17. He, D.; Hu, B.; Yao, Q. F.; Wang, K.; Yu, S. H. Large-Scale Synthesis of Flexible Free-Standing SERS Substrates with High Sensitivity: Electrospun PVA Nanofibers Embedded with Controlled Alignment of Silver Nanoparticles. *ACS Nano* **2009**, *3*, 3993–4002.
18. Baca, A. J.; Truong, T. T.; Cambrea, L. R.; Montgomery, J. M.; Gray, S. K.; Abdula, D.; Banks, T. R.; Yao, J. M.; Nuzzo, R. G.; Rogers, J. A. Molded Plasmonic Crystals for Detecting and Spatially Imaging Surface Bound Species by Surface-Enhanced Raman Scattering. *Appl. Phys. Lett.* **2009**, *94*, 243109.
19. Baca, A. J.; Montgomery, J. M.; Cambrea, L. R.; Moran, M.; Johnson, L.; Yacoub, J.; Truong, T. T. Optimization of Nanopost Plasmonic Crystals for Surface Enhanced Raman Scattering. *J. Phys. Chem. C* **2011**, *115*, 7171–7178.
20. Musick, M. D.; Keating, C. D.; Lyon, L. A.; Botsko, S. L.; Peña, D. J.; Holliway, W. D.; McEvoy, T. M.; Richardson, J. N.; Natan, M. J. Metal Films Prepared by Stepwise Assembly. 2. Construction and Characterization of Colloidal Au and Ag Multilayers. *Chem. Mater.* **2000**, *12*, 2869–2881.
21. Atwater, H. A.; Polman, A. Plasmonics for Improved Photovoltaic Bevices. *Nat. Mater.* **2010**, *9*, 205–213.
22. Nakanishi, H.; Bishop, K. J. M.; Kowalczyk, B.; Nitzan, A.; Weiss, E. A.; Tretiakov, K. V.; Apodaca, M. M.; Klajn, R.; Stoddart, J. F.; Grzybowski, B. A. Photoconductance and Inverse Photoconductance in Films of Functionalized Metal Nanoparticles. *Nature* **2009**, *460*, 371–375.
23. Stuart, H. R.; Hall, D. G. Island Size Effects in Nanoparticle-Enhanced Photodetectors. *Appl. Phys. Lett.* **1998**, *73*, 3815–3817.
24. Beck, F. J.; Polman, A.; Catchpole, K. R. Tunable Light Trapping for Solar Cells Using Localized Surface Plasmons. *J. Appl. Phys.* **2009**, *105*, 114310.
25. Catchpole, K. R.; Polman, A. Plasmonic Solar Cells. *Opt. Express* **2008**, *16*, 21793–21800.
26. Catchpole, K. R.; Polman, A. Design Principles for Particle Plasmon Enhanced Solar Cells. *Appl. Phys. Lett.* **2008**, *93*, 191113.
27. Nakayama, K.; Tanabe, K.; Atwater, H. A. Plasmonic Nanoparticle Enhanced Light Absorption in GaAs Solar Cells. *Appl. Phys. Lett.* **2008**, *93*, 121904.
28. Ferry, V. E.; Verschuuren, M. A.; Li, H. B. T.; Verhagen, E.; Walters, R. J.; Schropp, R. E. I.; Atwater, H. A.; Polman, A. Light Trapping in Ultrathin Plasmonic Solar Cells. *Opt. Express* **2010**, *18*, A237–A245.
29. Kang, M. G.; Xu, T.; Park, H. J; Luo, X. G.; Guo, L. J. Efficiency Enhancement of Organic Solar Cells Using Transparent Plasmonic Ag Nanowire Electrodes. *Adv. Mater.* **2010**, *22*, 4378–4383.
30. Xu, T.; Wu, Y. K.; Luo, X. G.; Guo, L. J. Plasmonic Nanoresonators for High-Resolution Colour Filtering and Spectral Imaging. *Nat. Commun.* **2010**, *1*, 59.
31. Kim, S.; Jin, J. H.; Kim, Y. J.; Park, I. Y.; Kim, Y.; Kim, S. W. High-Harmonic Generation by Resonant Plasmon Field Enhancement. *Nature* **2008**, *453*, 757–760.
32. Zijlstra, P.; Chon, J. W. M.; Gu, M. Five-Dimensional Optical Recording Mediated by Surface Plasmons in Gold Nanorods. *Nature* **2009**, *459*, 410–413.
33. Lipomi, D. J.; Ilievski, F.; Wiley, B. J.; Deotare, P. B.; Loncar, M.; Whitesides, G. M. Integrated Fabrication and Magnetic Positioning of Metallic and Polymeric Nanowires Embedded in Thin Epoxy Slabs. *ACS Nano* **2009**, *3*, 3315–3325.
34. Hu, A.; Guo, J. Y.; Alarifi, H.; Patane, G.; Zhou, Y.; Compagnini, G.; Xu, C. X. Low Temperature Sintering of Ag Nanoparticles for Flexible Electronics Packaging. *Appl. Phys. Lett.* **2010**, *97*, 153117.
35. Magdassi, S.; Grouchko, M.; Berezin, O.; Kamyshny, A. Triggering the Sintering of Silver Nanoparticles at Room Temperature. *ACS Nano* **2010**, *4*, 1943–1948.
36. Lu, Y.; Liu, G. L.; Lee, L. P. High-Density Silver Nanoparticle Film with Temperature-Controllable Interparticle Spacing for a Tunable Surface Enhanced Raman Scattering Substrate. *Nano Lett.* **2005**, *5*, 5–9.
37. Messina, E.; Cavallaro, E.; Cacciola, A.; Antonia Iatì, M.; Gucciardi, P. G.; Borghese, F.; Denti, P.; Saija, R.; Compagnini, G.; Meneghetti, M.; *et al.* Plasmon-Enhanced Optical Trapping of Gold Nanoaggregates with Selected Optical Properties. *ACS Nano* **2011**, *5*, 905–913.
38. Compagnini, G.; Patanè, G.; D'Urso, L.; Puglisi, O.; Cataliotti, R. S. On the Interaction of Carbon Nanowires with Noble

Metals through a Study of Their Surface-Enhanced Raman Spectra. *J. Phys. Chem. C* **2008**, *112*, 20301–20306.
39. Yang, J.; Wang, Z. Y.; Tan, X. B.; Li, J.; Song, C. Y.; Zhang, R. H.; Cui, Y. P. A Straightforward Route to the Synthesis of a Surface-Enhanced Raman Scattering Probe for Targeting Transferrin Receptor-Overexpressed Cells. *Nanotechnology* **2010**, *21*, 345101.
40. Fan, J. A.; Wu, C.; Bao, K.; Bao, J. M.; Bardhan, R.; Halas, N. J.; Manoharan, V. N.; Nordlander, P.; Shvets, G.; Capasso, F. Self-Assembled Plasmonic Nanoparticle Clusters. *Science* **2010**, *328*, 1135–1138.
41. Pietrobon, B.; McEachran, M.; Kitaev, V. Synthesis of Size-Controlled Faceted Pentagonal Silver Nanorods with Tunable Plasmonic Properties and Self-Assembly of These Nanorods. *ACS Nano* **2009**, *3*, 21–26.
42. Henzie, J.; Lee, J.; Lee, M. H.; Hasan, W.; Odom, T. W. Nanofabrication of Plasmonic Structures. *Annu. Rev. Phys. Chem.* **2009**, *60*, 147–165.
43. Tao, A. R.; Ceperley, D. P.; Sinsermsuksakul, P.; Neureuther, A. R.; Yang, P. D. Self-Organized Silver Nanoparticles for Three-Dimensional Plasmonic Crystals. *Nano Lett.* **2008**, *8*, 4033–4038.
44. Gupta, S.; Agrawal, M.; Uhlmann, P.; Simon, F.; Stamm, M. Poly(N-isopropyl acrylamide)-Gold Nanoassemblies on Macroscopic Surfaces: Fabrication, Characterization, and Application. *Chem. Mater.* **2010**, *22*, 504–509.
45. Fan, M.; Andradec, G. F. S.; Alexandre, G. B. A Review on the Fabrication of Substrates for Surface Enhanced Raman Spectroscopy and Their Applications in Analytical Chemistry. *Anal. Chim. Acta* **2011**, *693*, 7–25.
46. Wan, D.; Chen, H. L.; Lai, Y. T.; Yu, C. C.; Lin, K. F. Use of Reversal Nanoimprinting of Nanoparticles to Prepare Flexible Waveguide Sensors Exhibiting Enhanced Scattering of the Surface Plasmon Resonance. *Adv. Funct. Mater.* **2010**, *20*, 1742–1749.
47. Zou, X. Q.; Dong, S. J. Surface-Enhanced Raman Scattering Studies on Aggregated Silver Nanoplates in Aqueous Solution. *J. Phys. Chem. B* **2006**, *110*, 21545–21550.
48. Jin, R. C.; Cao, Y. W.; Mirkin, C. A.; Kelly, K. L.; Schatz, G. C.; Zheng, J. G. Photoinduced Conversion of Silver Nanospheres to Nanoprisms. *Science* **2001**, *294*, 1901–1903.
49. Aherne, D.; Ledwith, D. M.; Gara, M.; Kelly, J. M. Optical Properties and Growth Aspects of Silver Nanoprisms Produced by a Highly Reproducible and Rapid Synthesis at Room Temperature. *Adv. Funct. Mater.* **2008**, *18*, 2005–2016.
50. Pastoriza-Santos, I.; Liz-Marzán, L. M. Colloidal Silver Nanoplates. State of the Art and Future Challenges. *J. Mater. Chem.* **2008**, *18*, 1724–1737.
51. Tang, B.; Xu, S. P.; An, J.; Zhao, B.; Xu, W. Q. Photoinduced Shape Conversion and Reconstruction of Silver Nanoprisms. *J. Phys. Chem. C* **2009**, *113*, 7025–7030.
52. Zhang, X. Y.; Hu, A.; Wen, J. Z.; Zhang, T.; Xue, X. J.; Zhou, Y.; Duley, W. W. Numerical Analysis of Deep Sub-Wavelength Integrated Plasmonic Devices Based on Semiconductor-Insulator-Metal Strip Waveguides. *Opt. Express* **2010**, *18*, 18945–18959.
53. Zhang, X. Y.; Hu, A.; Zhang, T.; Xue, X. J.; Wen, J. Z.; Duley, W. W. Subwavelength Plasmonic Waveguides Based on ZnO Nanowires and Nanotubes: A Theoretical Study of Thermo-Optical Properties. *Appl. Phys. Lett.* **2010**, *96*, 043109.
54. Lynch, D. W.; Hunter, W. R. In *Handbook of Optical Constants of Solids Vol. 1*; Palik, E. D., Ed.; Academic: New York, 1985; pp 353−357.
55. Chen, J. G.; Zhang, T.; Zhu, J. S.; Zhang, X. Y.; Zhou, J. L.; Fan, J. F.; Hu, G. H. Low-Loss Planar Optical Waveguides Fabricated from Polycarbonate. *Polym. Eng. Sci.* **2009**, *49*, 2015–2019.
56. Blackie, E. J.; Le Ru, E. C.; Etchegoin, P. G. Single-Molecule Surface-Enhanced Raman Spectroscopy of Nonresonant Molecules. *J. Am. Chem. Soc.* **2009**, *131*, 14466–14472.